3.3 Our method

Our method resembles the human approach to image matching in the sense that we also employ as guidelines features common to both images. It seems natural not to restrict the comparison to the bifurcation points, but to use instead the more significant structures visible in the image, that is, the vessel tree. Opposite to the bifurcation points approach [9, 118], ours does not have such a strong dependence of the quality of the segmentation. In this sense, our method can be considered similar to that of Pinz et al [75].

The main goal for this chapter was to redesign the algorithm already used for CT to MR registration to suit any modality of ophthalmologic image. In principle, the registration in 2-D is far easier to perform:

- images are one order of magnitude faster to process and store.
- the search space is much smaller: only 1 rotation and two translation parameters.
- volumes or surfaces require complex visualisation algorithms, which are not necessary in 2–D.

However, as we commented in the introduction of this chapter, we had to process not only one-to-one image registrations, but also many-to-one for the *SLO* case. Actually, the sequences of *SLO* images were stored in CD-ROMs as they contained from one thousand to three thousand images. New constraints must be dealt with:

- the time spent for each frame becomes important, since it is multiplied thousands of times for the total sequence.
- the resulting transformation from one frame is likely to be a good initial guess for the next one.
- but at a certain times, image contents vary a lot with regard to the preceding frame.
- the algorithm will inevitably fail for a number of frames due to two reasons: the processed image is far too dissimilar from the reference, or because of failures in the acquisition process. Specifically, movements of the head and eye place the camera out of field.
- since the acquisition comprises a wide period of time, chances are that the translation parameters to compute are broader than with the other modalities. In fact, our results will show they may raise up to one third of the image.

Although most of the chapter is devoted to sequence *SLO* registration, we have applied successfully the method to a large database of images as listed in table 3.2.

Modality	Images per study	Number of studies
Stereo angiographies	2	49
Temporal	2	48
Green to retinography	2	10
Temporal sequence	1000 to 3000	3

Table 3.2: Outline of retinographies in the database.

Perfect segmentation of the whole vessel tree is not an easy task because images often provide poor contrast and vessels vary in diameter and intensity level; some papers are dedicated to this sole purpose [66, 99]. However, we were fortunate to have already addressed a similar problem for CT and MR brain registration. For this purpose, we developed a precise and reliable detector of the creaseness (ridgeness or valleyness) of an image. We already described this operator in section 2.2.

Compared to the CT and MR volumes processed in the last section, *SLO* images have some new properties which must be considered. One which will be relevant at the results sections, when comparing the evolution of the grey level for a registered sequence, is the low signal-to-noise ratio. The noise in the grey level of retinographies is caused by the optical nature of the acquiring devices: the light they measure must travel from and to the retina, which actually is a set of translucent tissues difficult to model. Additional noise is originated at the grabbing of the images from the original analogic source.

We have examined the images to study the nature of the noise: in figure 3.4 (top), we took a window containing only background information, and made a histogram of the values contained. The histogram, as shown in the below figure, is well approximated by a Gaussian of mean $\eta = 68.5$ and standard deviation $\sigma = 9.12$. This Gaussian bell, taken for each pixel for its intensity values, must not be confused with the smoothing convolution of the image when computing the derivatives. Results were similar for other frames and sequences.

A similar, though much detailed, conclusion can be driven from [50]. In this paper, Lois evaluates the repeatability of the background fundus measurements in *SLO* images, with a group of 10 patients plus 10 normal volunteers. After manual selection of background values by an expert ophthalmologist, she observes differences in the ranges $(1.4, 13.5)$ for volunteers and $(1.5, 9.3)$ for patients. Therefore we must conclude that before using any raw value taken from the original image, it is convenient to convolve the image with a Gaussian Kernel in order to get rid of some noise amplitude. This is the same smoothing needed when computing the derivatives.

After vessels have been extracted, we needed to choose a scheme to transform iteratively the images until they become aligned. In literature many methods to measure the alignment exist; we could, for instance, segment each branch and follow some heuristic to choose its corresponding. Its drawback is the same as bifurcation methods have: the extra segmentation step is prone to propagate its errors to the optimisation step. Therefore, we choose the well-known cross-correlation between the two images. This measure is fast and also, as we require, it matches common

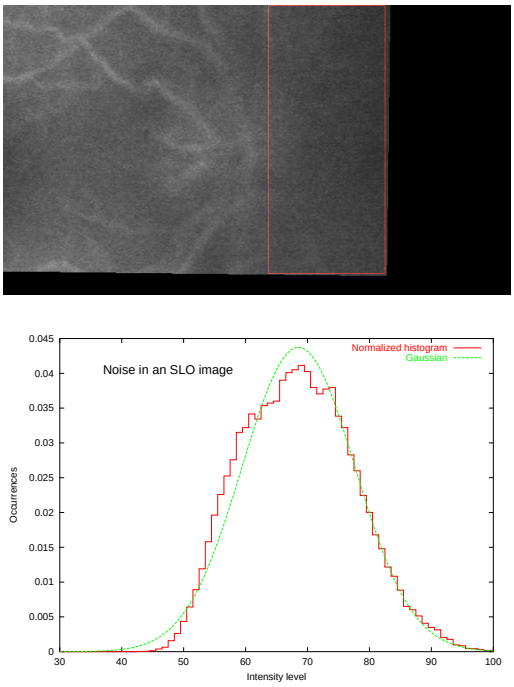

Figure 3.4: *SLO* images are very noise. The histogram of a sample of the background can be well modelled with a Gaussian bell of standard deviation $\sigma = 9.12$.

extracted features despite of missing or spurious data.

We have implemented the iterative Simplex algorithm to optimise the alignment process, and added an initial wide search to improve its robustness. The optimisation process is fully described in section 3.3.

Figure 3.5 summarises graphically the steps forming our algorithm. Each step has been numbered in a circle as ①, and consist, in short, in:

① Extract the creaseness images.

② Build a hierarchical pyramid for each image.

③ Find the best candidates with exhaustive search.

④ Refine each seed through the image hierarchy.

⑤ Re-run ④ with the best result to include scaling

These steps have been further developed in pseudo-code in figures 3.6 and 3.7. Through the following sections, numbers labelled as ① refer to this scheme.

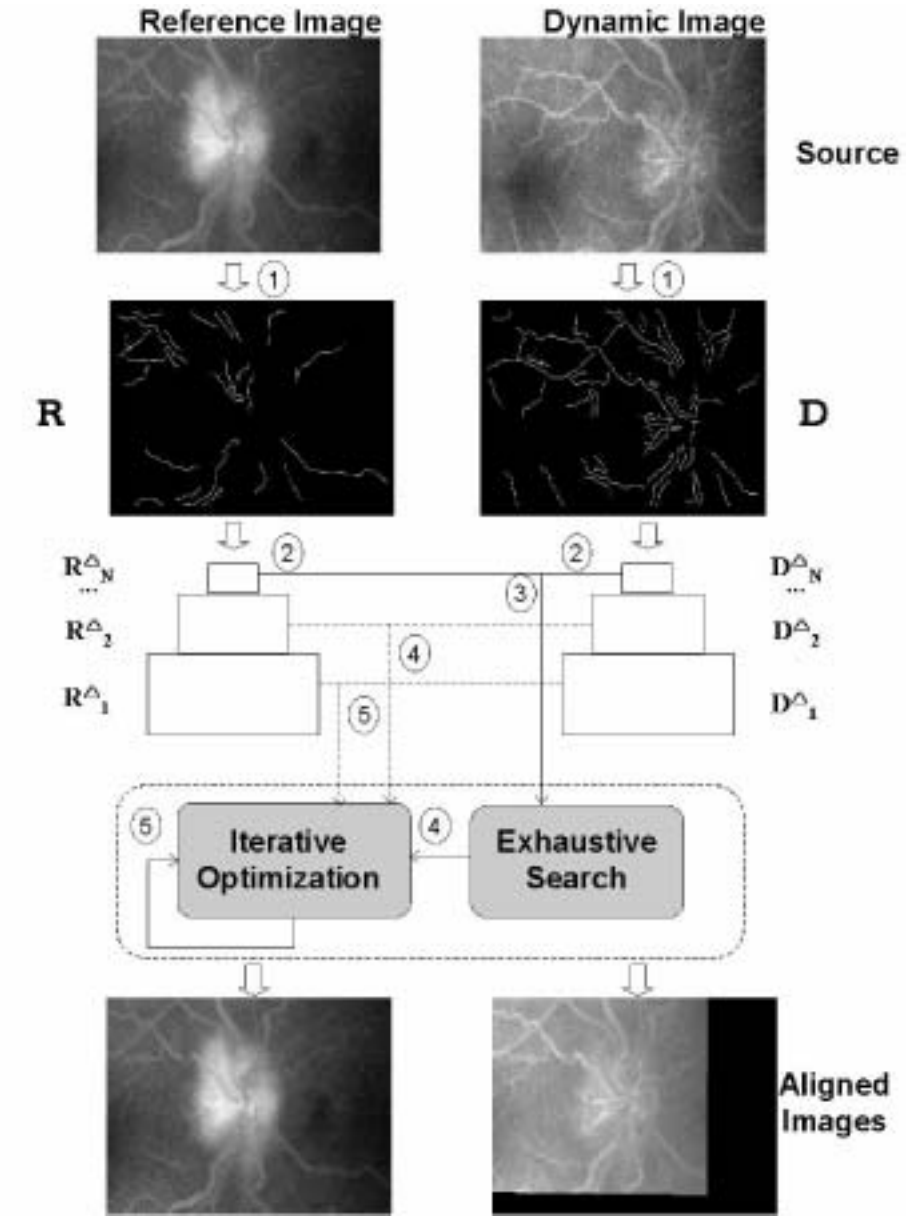

Figure 3.5: Graphic scheme of the alignment procedure.

$\mathbf{R}$, $\mathbf{D}$	reference and dynamic images
$\mathbf{N}$	number of pyramid levels (1 bottom, $\mathbf{N}$ top)
S_l	set of $\#S_l$ best translation and rotation seeds at level l, $1 \leq l \leq \mathbf{N}$
SimplexRefine(A, B, Seed, tolerance)	Run the iterative Simplex algorithm with the Seed on the images A and B until the given tolerance threshold is achieved

Notation

① Extract the creaseness images with Gaussian window α, and prune results for crests shorter than l_{min} pixels.

$\mathbf{R}$= Prune(Crest($\mathcal{R}$, α), l_{min});
$\mathbf{D}$= Prune(Crest($\mathcal{D}$, α), l_{min});

② Build a hierarchical pyramid for each image.

```
function BuildLevel (image A) {
 NewLevel = NewImage(Width(A)/2, Height(A)/2);
 for i=1 to Width(NewLevel)
  for j=1 to Height(NewLevel)
   NewLevel[i,j] = Max(A_{2i,2j}, A_{2i+1,2j},A_{2i,2j+1}, A_{2i+1,2j+1});
 return Newlevel;
}
function BuildPyramid(image A) {
 Pyramid[1] = CopyImage(A);
 for i = 2 to N {
  Pyramid[i] = BuildLevel(Pyramid[i-1]);
  }
 return Pyramid[];
}
R^△= BuildPyramid(R);
D^△= BuildPyramid(D);
```

③ Find the list of best seeds S_N at the top level for a range $[-r, r]$ of candidate rotation angles.

```
S_N = ∅;
for α = −r to r step s {
 D_α =Rotate(D^△[N], α);
 C = FFT^{-1}(FFT(R^△[N]) · FFT(D_α));
 S_N = S_N ∪ TopValues(C);
}
```

Figure 3.6: Pseudo-code of the registration algorithm (1)

④ Refine each seed through the image hierarchy.

```
for l = N − 1 to 1 {
  S_l = {};
  for i = 1 to #S_{l+1} {
    S_l = S_l ∪ SimplexRefine(R^△[l], D^△[l], S_{l+1}[i],tolerance);
  }
}
```

⑤ Re-run ④ with the best result within S_1, this time including scaling parameters.

⑥ Divide registered images in grids, and apply the registration algorithm separately to each resulting pair.

Figure 3.7: Pseudo-code of the registration algorithm (2)

3.3.1 Creaseness measures

Vessels are reliable landmarks in retinal images because they are almost rigid structures and they are depicted in all modalities. As we have reported in the introduction, all cited papers except one use them for this purpose.

Little work was necessary to adapt the operator lready defined in 2.2 to 2–D ophthalmologic images. The first item was to consider whether to extract creases or valleys; vessels show as one or the other depending on the modality. Moreover, in time sequences it can be seen their change from low to high values, this is to say, from valley-like to crease-like shapes, as contrast flows in. After a peak value, the inverse process takes places and they return to the original low values. Figure 3.8 illustrates this process. Taking this into account, we resolved to use the creaseness value in absolute value as input for the registration step, i.e., we discard the information regarding their creaseness or valleyness.

The creaseness operator must be tuned with a short number of parameters. We took the choices specified in table 3.3.

Size of the smoothing Gaussian	3.5 pixels
Size of the integration window	5 pixels
Enhancing factor	0.1
Threshold	0.25
Minimal crease length	100 pixels

Table 3.3: Parameters to extract the creases.

This choice performed well for all the modalities, thus we decided not to include them in our battery of tests for validation. A reasonable modification would be to make the enhancing and the threshold factor depend on the quality of the image: less contrasted images could work better with other values. But the additional computation would benefit solely a small number of frames belonging to the begining of the sequence and therefore we decided to pospone the actual implementation of this improvement to a further develoment step.

The creaseness images as defined here were suitable for registration of images from all modalities. However, for the *SLO* , sequences, sometimes the search was missguided by the high number of features extracted. A further step was necessary, and it consisted on the prunning of the creases extracted, in order to keep only those most relevant, longer than a given threshold (recall figure 3.9 for a sample). Again, this can be discussed to be an arbitrary choice, for any value ought to be validated in the battery tests. However, and similarly to the choices at the previous paragraph, since the method ran well we did not include its validation in our experiments. Figure 3.3 ilustrates this process for an example image.

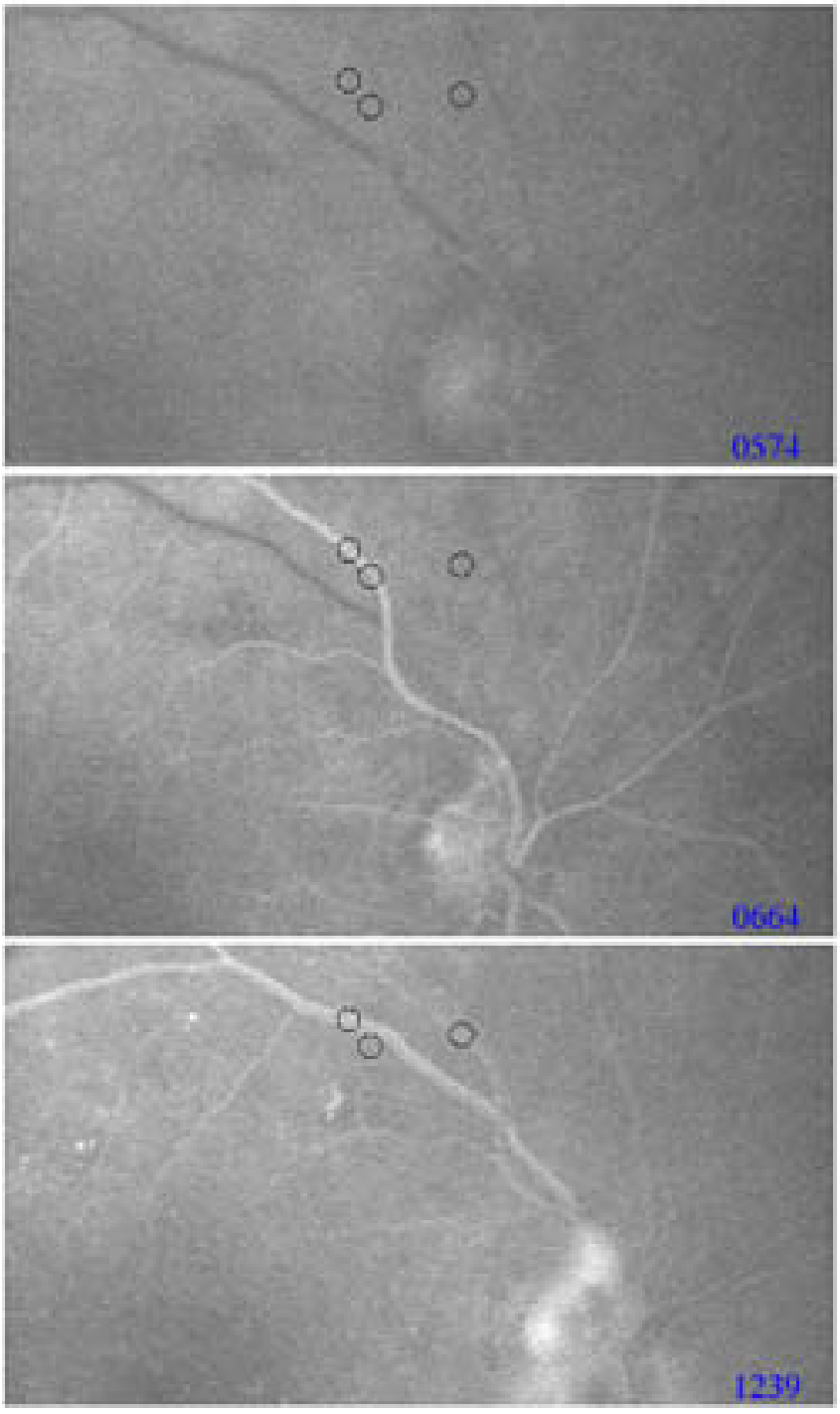

Figure 3.8: Vessels change their brightness along the sequence. The artery, marked with a circle, is not visible in the top frame, has maximum brightness in the middle one and again barely visible in the bottom one.

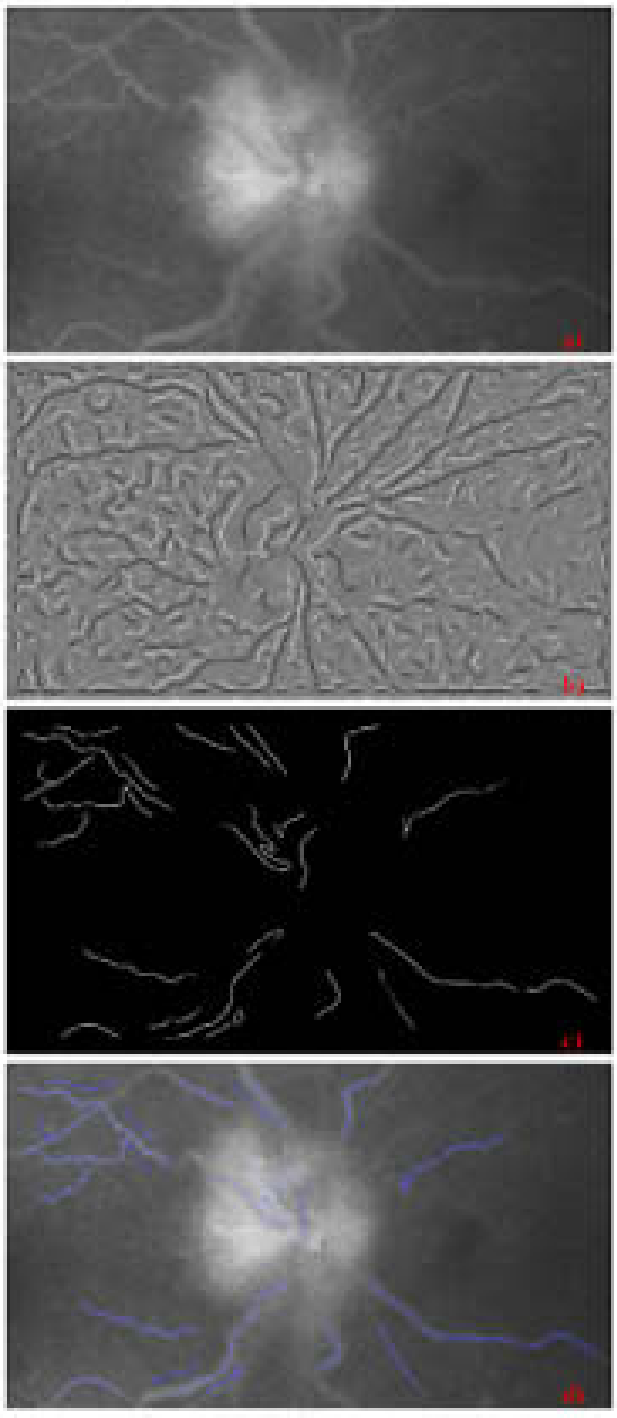

Figure 3.9: a): reference *SLO* image for patient A, b) Raw creaseness image, c) Creases after prunning shorter than 100 pixels, d) Composition of a) with c) in blue.